Original Paper

Brain, Behavior and Evolution

Brain Behav Evol 2014;83:181–198
DOI: 10.1159/000357750

Received: November 8, 2012
Accepted after second revision: December 4, 2013
Published online: March 24, 2014

Do American Goldfinches See Their World Like Passive Prey Foragers? A Study on Visual Fields, Retinal Topography, and Sensitivity of Photoreceptors

Patrice E. Baumhardt Bret A. Moore Megan Doppler
Esteban Fernández-Juricic

Department of Biological Sciences, Purdue University, West Lafayette, Ind., USA

Key Words
Binocular vision · Ganglion cells · Oil droplets · Photoreceptors · Retinal topography · Visual fields

Abstract
Several species of the most diverse avian order, Passeriformes, specialize in foraging on passive prey, although relatively little is known about their visual systems. We tested whether some components of the visual system of the American goldfinch *(Spinus tristis),* a granivorous bird, followed the profile of species seeking passive food items (small eye size relative to body mass, narrow binocular fields and blind areas, centrally located retinal specialization projecting laterally, ultraviolet-sensitive vision). We measured eye size, visual field configuration, the degree of eye movement, variations in the density of ganglion cells and cone photoreceptors, and the sensitivity of photoreceptor visual pigments and oil droplets. Goldfinches had relatively large binocular (46°) and lateral (134°) visual fields with a high degree of eye movement (66° at the plane of the bill). They had a single centrotemporally located fovea that projects laterally, but can be moved closer to the edge of the binocular field by converging the eyes. Goldfinches could also increase their panoramic vision by diverging their eyes while handling food items in head-up positions. The distribution of photoreceptors indicated that the highest density of single and double cones was surrounding the fovea, making it the center of chromatic and achromatic vision and motion detection. Goldfinches possessed a tetrachromatic ultraviolet visual system with visual pigment peak sensitivities of 399 nm (ultraviolet-sensitive cone), 442 nm (short-wavelength-sensitive cone), 512 nm (medium-wavelength-sensitive cone), and 580 nm (long-wavelength-sensitive cone). Overall, the visual system of American goldfinches showed characteristics of passive as well as active prey foragers, with a single-fovea configuration and a large degree of eye movement that would enhance food searching and handling with their relatively wide binocular fields.

Introduction

Birds are highly visual organisms that live in a broad range of environmental conditions. Their complex visual systems [i.e. large eyes, wide visual fields, 4 types of visual pigments, oil droplets to enhance color discrimination, etc.; Cuthill, 2006] are tuned to optimize the gathering of sensory information to find food, detect predators, and reduce sun glare in different environmental conditions [Martin, 2007].

KARGER

E-Mail karger@karger.com
www.karger.com/bbe

0006–8977/14/0833–0181$39.50/0

Esteban Fernández-Juricic
Department of Biological Sciences
Purdue University, Lilly Hall G-302
915 W. State Street, West Lafayette, IN 47907 (USA)
E-Mail efernan@purdue.edu

The avian visual system has been proposed to vary depending on whether the main prey is passive (e.g. seeds, fruits) or active (e.g. insects, vertebrates). The rationale is that the detection and tracking of active prey would require some visual adaptations to increase encounter and capture rates [reviewed in Cronin, 2005]. In the most diverse avian order, Passeriformes, many species mainly forage on passive food items that are detected and captured at close distances [Elphick et al., 2001], yet comparatively little is known about their visual systems [but see Rahman et al., 2006; Dolan and Fernández-Juricic, 2010; Fernández-Juricic et al., 2011b]. We studied a Passeriform of the Fringillidae family, the American goldfinch (*Spinus tristis* Linnaeus, 1758), to assess whether its visual system follows the profile of species seeking passive prey. American goldfinches are almost entirely granivorous and sexually dimorphic, particularly during the breeding season [McGraw and Middleton, 2009]. They inhabit open habitats (fields, floodplains, cultivated pastures) but can also be seen in backyards (i.e. frequent visitors of bird feeders) and orchards [McGraw and Middleton, 2009].

The way birds perceive visually is the result of different types of visual information being gathered simultaneously (e.g. overall and localized visual resolution, motion detection, binocular overlap, color vision). In this study, we were able to investigate 5 visual properties of American goldfinches: (1) eye size; (2) variations in the density of ganglion cells and cone photoreceptors across the retina to determine the position of areas specialized in acute vision (e.g. fovea), chromatic and achromatic vision, and motion detection; (3) the sensitivity of the visual pigments and oil droplets involved in color vision; (4) the configuration of the visual fields (the extent of the binocular and lateral fields and blind area), and (5) the degree of eye movement. In the next paragraphs, we review the main hypotheses accounting for the differences in the visual systems of species that catch passive versus active prey and develop specific predictions for American goldfinches.

Visual acuity or visual resolution is determined by eye size (i.e. overall visual resolution) and the peak density of retinal ganglion cells (i.e. localized visual resolution) [Pettigrew et al., 1988]. The bigger the eye, the larger the area over which the image spreads on the retina, activating a greater number of photoreceptors and hence increasing the overall visual resolution [Martin, 1993; Kiltie, 2000]. Species that feed on active prey tend to have larger eyes relative to their body mass (allowing them to detect prey from farther away) than species that feed on passive prey (which generally detect prey at relatively close distances) [Garamszegi et al., 2002; Lisney and Collin, 2007]. Therefore, we predicted that American goldfinches would have relatively smaller eyes in relation to their body mass compared to other bird species.

Photoreceptors gather information from the environment and, after processing it in the outer and inner retina, ganglion cells transfer it to the visual centers of the brain [McIlwain, 1996]. The distribution of ganglion cells across the avian retina is quite heterogeneous [Walls, 1942; Meyer, 1977]. Some types of retinal specializations consist of areas in the retina with a high density of specific cell types, which may correspond with the centers for acute vision. For instance, retinal specializations like the fovea, visual streak, and area have a high density of photoreceptors and retinal ganglion cells compared to the retinal periphery [Meyer, 1977]. In general, species that hunt active prey, like falcons, hawks, owls, and flycatchers, have been reported to have higher cell densities in their retinal specializations (and in some cases more than one retinal specialization per retina) than species that feed on passive prey [e.g. Reymond, 1985, 1987; Coimbra et al., 2006, 2009; Dolan and Fernández-Juricic, 2010; Fernández-Juricic et al., 2011a; Lisney et al., 2012]. Consequently, we predicted that American goldfinches would have a single fovea with a relatively low density of retinal ganglion cells compared to species which forage on active prey. We also predicted that the distribution of cone photoreceptors would match that of the retinal ganglion cells [e.g. Querubin et al., 2009; Moore et al., 2012], being higher around the fovea than in the retinal periphery, although little is known about cell density covariations at these two retinal layers in Passeriformes.

Many of the Passeriformes studied to date that forage on a combination of passive and active prey have been found to possess an ultraviolet-sensitive (UVS) visual pigment variant [Ödeen and Håstad, 2003; Hart and Hunt, 2007; Bowmaker, 2008; Ödeen et al., 2011]. However, raptors that specialize in active prey have been shown to have a violet-sensitive (VS) visual pigment variant [Ödeen and Håstad, 2003], although the perceptual reasons behind these differences are still unclear. Therefore, we predicted that the American goldfinch would have a UVS visual system which could increase their ability to discriminate seeds and fruits that reflect UV from the background [Tovée, 1995], as well as to assess the quality of potential mates since parts of their plumage (e.g. yellow feathers) reflect in the UV [MacDougall and Montgomerie, 2003].

The visual field configuration [i.e. the volume of space around the head from which an animal can perceive visually; Martin, 1993] has also been shown to vary between vertebrate predators and prey; species feeding on active prey tend to have wider binocular fields and blind areas, whereas those feeding on passive prey tend to have narrower binocular and blind areas to increase lateral vision and enhance predator detection [Hughes, 1977]. This visual field configuration is associated with the position of the orbits in the skull and the retinal specialization. Species foraging on active prey tend to have high degrees of orbit convergence, whereas those foraging on passive prey tend to have laterally placed orbits [Heesy and Hall, 2010]. Thus, we predicted that American goldfinches would have relatively narrow binocular fields and blind areas, which would increase the size of the lateral visual fields, and a limited degree of eye movement characteristic of many birds [Martin, 1993].

Methods

American goldfinches were captured in Tippecanoe County, Ind., USA, from March 2010 to February 2012 using hanging finch traps and mist nets. Individuals were housed in 0.61 × 0.61 × 0.76 m cages in an indoor room on a 12-hour light/dark cycle in the animal facilities at the Purdue University campus. Capture, handling, and euthanasia (when performed) were approved under Purdue Animal Care and Use Committee protocols 09-018 and 10-012.

Visual Field Configuration

The visual field configuration of the American goldfinch was measured in 8 individuals using an ophthalmoscopic reflex technique [Martin, 1984]. We measured a total of 8 individuals when the eyes were at rest, 6 of which were also measured when the eyes converged/diverged (see details below). Individual goldfinches were restrained in a horizontal position in the center of a visual field apparatus with their bills attached to a holder. The bill was held at the angle that was characteristic of goldfinches in a vigilant posture, which was determined from pictures of animals in the wild. We used an angular coordinate system to measure the visual fields and placed the head in the center of a spherical space, with the horizontal axis of the sphere running through the eyes of the individual. In this coordinate system, 90° corresponded to the position in front of the head, 0° corresponded to the position directly above the head, and the 270° corresponded to the position behind the head. We defined the plane connecting 90° to 270° as the horizontal plane parallel to the ground [Martin, 1986]. We measured the extent of the retinal projection into the spherical space [Martin, 2007]. We corrected these measurements following Martin [1984] so that they took into account the distance between the ophthalmoscope and the eye of the subject. Measurements were taken in 10° increments from 140 to 270° around the head with an accuracy of ±0.5° with a Keeler Professional ophthalmoscope. We did not measure from 130 to 260° underneath the head due to obstruction of the eyes by either the body or the visual field apparatus.

We measured the visual fields while birds were (1) at rest and (2) converging or diverging their eyes [Martin, 2007]. When the eyes were at rest (they were not following the movement of the ophthalmoscope), we also measured the projection of the pecten, which is a vascularized area in the avian retina that does not have visual pigments. We elicited eye movements (convergent, divergent) by providing a visual (i.e. flashing light) or auditory (i.e. jingling keys) stimulus in front of or behind the head of the individual. The sizes of the lateral [360 – (mean blind field + mean binocular field)/2], binocular, blind, and cyclopean (binocular + lateral right + lateral left visual areas) fields were calculated following Fernández-Juricic et al. [2008].

Retinal Ganglion Cell Density and Distribution

We measured the eye axial length from the anterior portion of the cornea to the most posterior portion of the back of the eye (in mm). We hemisected the eye anterior to the ora serrata to keep the retina undamaged using a razorblade and removed the vitreous humor with tweezers and spring scissors. In our experience, the use of a razorblade versus the scalpel blade eye rotation method traditionally used in Stone [1981] provides a smoother, gentler method for accessing the retinal tissue with less chance of damage [see also Ullmann et al., 2012]. We removed the vitreous humor at this stage because it dehydrates more than the retina, so keeping it could have caused distortion of the retinal tissue. Extraction of the retina was performed by detaching the choroidal layer from the sclera and severing the optic nerve head, following Ullmann et al. [2012]. After extraction, we very carefully removed the choroid or loose fragments of pigmented epithelium with either tweezers or a small paintbrush while the tissue was bathed in phosphate-buffered saline (PBS) solution (pH 7.2–7.4, ~310 mOsm/kg). We made sure that the use of a paintbrush did not cause any mechanical damage to the retinal tissue. However, this is a potential caveat when wholemounting the retina.

We then placed the retina in PBS with 4% paraformaldehyde for 24 h to fix the tissue. After fixation, the retina was washed in PBS, and subsequently placed into a bleaching solution of 5% hydrogen peroxide for 5 days to remove any pigment in the remaining epithelial cells. The retina was then washed in PBS and flattened on a gelatinized slide [Stone, 1981; Ullmann et al., 2012]. The pecten was removed prior to flattening to enable the retina to lie completely flat on the slide [Lisney et al., 2012, 2013]. Additionally, this method minimized problems with asymmetric shrinkage across the retina [Ullmann et al., 2012] that could become prevalent if certain points of the retina remained partially adhered to the ora serrata or the area around the pecten. The retina was heat-fixed onto the slide by placing it in a vessel containing 4 drops of formalin and heated to 60°C for 2 h. After heat fixation, the retina remained in this chamber for another 24 h. We took pictures of the retina with a Panasonic Lumix FZ28 digital camera to account for tissue shrinkage [Ullmann et al., 2012].

The staining process began by clearing the retina in Histo-Clear (National Diagnostics) in two 10-min rinses totaling 20 min, followed by two 2-min rinses in the following solutions: 100% ethanol twice, 95% ethanol acidified with glacial acetic acid, 80% ethanol, 70% ethanol, and distilled water acidified with glacial acetic acid. We then immersed the retina in 0.25% cresyl violet for 12 min and immediately rinsed it with acidified distilled water, and then dehy-

drated it in 70 and 80% ethanol for 30 s each. We placed the retina in 95% ethanol acidified with glacial acetic acid for 60 s, followed by two 60-second rinses in 100% ethanol. Finally, we placed the retina in Histo-Clear for two 10-min rinses [Stone, 1981; Ullmann et al., 2012]. We added Permount (Fisher Scientific) over the retina, placed a coverslip on it, and allowed it to dry. Once the slide had dried, an additional picture was taken to complete tissue shrinkage estimations. To account for tissue shrinkage, the area of the retina before and after staining was measured using ImageJ (http://rsb.info.nih.gov/ij/).

To sample the ganglion cells on retinal, cresyl violet-stained wholemounts, we followed some of the procedures of Coimbra et al. [2009], who used for the first time a stereological approach by considering the ganglion cell layer as a single section. The perimeter of the retina was first traced using Stereo Investigator 9.13 (MBF Bioscience) with a ×4 objective and a 0.10 aperture on an Olympus BX51 microscope. We used the SRS Image Series Acquire module to apply an orderly grid over the traced retina using the following parameters: area sampling fraction (asf; the ratio of the area of the counting frame to the area of the grid) = 0.02 ± 0.001 per retina, thickness sampling factor (tsf; the ratio of the height of the dissector to the mean measured thickness) = 1 per retina, and ΣQ^- (the sum of the total number of neurons counted) = 15,749 ± 1,489 per retina [West et al., 1991; Bonthius et al., 2004]. The grid size per retina set by Stereo Investigator was, on average, 359.8 ± 8.0 × 360.5 ± 11.5 μm.

The coefficient of error (CE) is a statistical method for determining the accuracy of a stereological estimate of a cell population size, with CE <0.1 considered to be highly reliable [Glaser and Wilson, 1998; Slomianka and West, 2005; Coimbra et al., 2009]. We estimated the Scheaffer-Mendenhall-Ott (SMO) CE in two different ways depending on the type of counting. We counted 1 retina 'live' focusing on a single plane with the optical fractionator workflow in Stereo Investigator, which provided the SMO CE (table 1). We also counted 2 retinae with ImageJ using photomicrographs acquired in the SRS Image Series Acquire module of Stereo Investigator, which does not output the SMO CE. For these two retinae, we manually estimated the SMO CE (table 1) [equations A4a, A4b, and A5 for random populations in Glaser and Wilson, 1998]. The live and manual estimates had similar SMO CE (all <0.1; table 1). We also used another means of determining the reliability of our estimates by manually calculating the SMO CE^2/CV^2 ratio (where CV is the coefficient of variation) for these three retinae. This ratio indicates whether the variance created by using stereology accounts for less than 50% (or <0.5) of the observed variance of the cell population [Slomianka and West, 2005]. All three retinae had SMO CE^2/CV^2 ratios <0.01 (table 1), which is substantially lower than the accepted value of 0.5 used in other studies [Slomianka and West, 2005]. The results of these two indices show that our cell counts were reliable.

A mean of 408.7 ± 1.67 grid sites per retina was used; however, not all could be counted because of counting frames being outside of the retina, a lack of focus on some retinal sectors, and small retinal tears. In the upper left hand corner of each grid, a 50 × 50 μm counting frame was placed to avoid double counting of cells. At each counting frame, we took a picture with an Olympus S97809 microscope camera on the plane at which the highest resolution and contrast could be attained using the microscope focus with a ×100 oil immersion objective and a 1.30 aperture. These images were then captured using SnagIt (www.tech-smith.com/Snagit). We counted ganglion cells that were fully encompassed within the counting frame, as well as cells that were touching the upper and right edges of the counting frame, but excluded cells touching the lower and left edges of the counting frame, following Gundersen [1977]. In a limited number of cases when part of the photomicrograph was not in good condition (e.g. presence of some pigmented epithelium), we divided the counting frame into 4 equal quadrats. We counted in only those quadrats where cells were clearly visible, and corrected for the smaller counting area in the calculation of cell density following Dolan and Fernández-Juricic [2010].

The avian retina is a complex, multilayered tissue in which retinal ganglion cells can be found at multiple sublaminae as the density of cells increases, specifically around the perifoveal region [Moroney and Pettigrew, 1987; Coimbra et al., 2006, 2009]. One of the potential shortcomings of our ganglion cell counting method is that we could have missed a substantial fraction of the cells by using a single plane. To investigate this, we performed a cross section of a cresyl violet-stained wholemounted retina from another Passerine bird: the European starling *(Sturnus vulgaris)*. We placed the slide containing the wholemounted retina back into a xylene solution to remove the toluene-based coverslipping agent, removed the coverslip, and cut out a portion of the retina with a razor blade. We mounted this portion in paraffin and cross-sectioned the retina with a microtome, which was placed onto a slide without further staining. In the cross section, we measured the thickness of the ganglion cell layer after processing in different parts of the perifoveal region, yielding an average of 4.5 ± 0.11 μm (n = 15 samples). In another wholemounted cresyl violet-stained starling retina, we measured the z-depth of the retinal ganglion cell layer with Stereo Investigator from the vitreal side of the ganglion cell layer to the beginning of the inner plexiform layer. The z-depth measurements showed a thickness in this preparation of 5.3 ± 0.73 μm (n = 19). We took photomicrographs at sites in the perifoveal region of the retina, focusing on a single plane approximately in the center of the ganglion cell layer. Next, we took photomicrographs while focusing on different planes within a given site and counted the retinal ganglion cells for each image. We found that the single plane photomicrograph captured most (93.37 ± 1.36%; n = 10) of the ganglion cells. Consequently, we believe that our sampling method was able to account for a large proportion of retinal ganglion cells even in the perifoveal areas with multiple ganglion cell layers.

There are different criteria to count retinal ganglion cells [discussed in Lisney et al., 2012]. Because cresyl violet also stains other types of cells, such as amacrine and glial cells, some authors count all cells without distinguishing among them [e.g. Coimbra et al., 2006]. However, we followed other studies [Hughes, 1977; Freeman and Tancred, 1978; Ehrlich, 1981; Stone, 1981; Rahman et al., 2006] where retinal ganglion cells are distinguished based on cell shape, soma size, Nissl body accumulation in the cytoplasm, and staining of the nucleus. Details on the criteria we used are presented in online supplementary appendix 1 (for all online suppl. material, see www.karger.com/doi/10.1159/000357750).

We counted the retinal ganglion cells at each site of the retina with ImageJ (http://rsb.info.nih.gov/ij/). The area counted in each picture was 0.0025 mm^2. We corrected for tissue shrinkage by taking 0.0025 + (0.0025 × proportion of shrinkage). This correction was performed on each retina, and the cell density (number of cells/mm^2) was calculated by dividing the number of cells by the

Table 1. Parameters used in the estimation of the accuracy of the cell counts (SMO CE and SMO CE^2/CV^2)

Retina No.	Cells Counted, n	SD of the cells counted	Sites counted, n	Mean cells per site, n	Variance	SMO CE	CV	SMO CE^2/CV^2
RGC 1	18,548	24.5	407	45.62[a]	597.86[a]	0.026[a]	0.538	0.00246
RGC 2	15,229	20.5	412	37.0	421.7	0.0274	0.556	0.00243
RGC 3	13,471	18.2	407	33.1	329.7	0.0272	0.549	0.00246
PH 4	10,961	47.0	250	43.8	2,212.7	0.0679	1.07	0.00400
PH 5	9,132	44.5	248	36.8	1,980.0	0.0767	1.21	0.00403
PH 6	18,527	58.0	248	74.7	3,362.1	0.0492	0.776	0.00403
PH 7	18,745	59.4	253	74.1	3,530.5	0.0504	0.802	0.00395
PH 8	12,296	46.3	253	48.6	2,147.3	0.0599	0.953	0.00395
PH 9	13,730	48.7	255	53.8	2,376.2	0.0567	0.905	0.00392

RGC = Retinal ganglion cells; PH = photoreceptors; SD = standard deviation. [a]Values given from the Stereo Investigator program on the retina that was counted 'live' in the program. All other values were calculated manually outside the Stereo Investigator program (see text for details).

corrected tissue area. Additionally, we calculated the total number of ganglion cells using the following equation: N total = $\Sigma Q^- \times 1/asf \times 1/tsf$ [Coimbra et al., 2006].

Topographic maps were built following Stone [1981] and Ullmann et al. [2012] to determine variations in retinal ganglion cell density across the retina. Isodensity lines were interpolated from adjacent density values. We used 6 cell density isodensity values (0–9,999; 10,000–18,999; 19,000–25,999; 26,000–28,999; 29,000–34,999, and ≥35,000 cells/mm^2).

We calculated visual acuity (or anatomical spatial resolving power) following Williams and Coletta [1987] and Pettigrew et al. [1988]. We first calculated the posterior nodal distance (PND) as 0.6 multiplied by the eye axial length [Martin, 1993; Ullmann et al., 2012], and the retinal magnification factor (RMF) was calculated as 2πPND/360 [Pettigrew et al., 1988]. We then estimated the visual acuity (cycles/degree), i.e. the highest spatial frequency that can be detected under optimal light conditions, as follows:

$$F_n = \frac{RMF}{2}\sqrt{\frac{2D}{\sqrt{3}}},$$

where D is the peak retinal ganglion cell density [Williams and Coletta, 1987].

We performed a histological cross section on one American goldfinch eye to corroborate the presence of a fovea. We immersed the hemisected eye cup in Bouin's fixative for 24 h and washed it in 0.01 M PBS. The area of the retina containing the fovea was then isolated by cutting a 2-mm-thick strip from the eyecup, which was then placed in 70% ethanol for 1 week to remove any excess Bouin's fixative. We then embedded the section of the retina containing the fovea in paraffin wax, followed by serial sectioning along the anterior-posterior axis with a Thermo Scientific Shandon Finesse ME microtome (Waltham, Mass., USA). Finally, we stained the tissue with hematoxylin/eosin in Thermo Scientific Shandon Varistain 24-3.

Photoreceptor Density and Distribution

We established variations in the density and distribution of photoreceptors across the retina by mapping the oil droplets. We successfully counted 6 retinae from 6 individuals. We removed the eyes and the retinae following the same procedures described above. The retina was bathed in PBS and subsequently flattened on a gelatinized slide and inverted to place the photoreceptor layer on top. The perimeter of the retina was first traced using Stereo Investigator 9.13 (MBF Bioscience) with a ×4 objective and a 0.10 aperture on an Olympus BX51 microscope. We used the SRS Image Series Acquire module to apply an orderly grid over the traced retina using the following parameters: asf = 0.0095 ± 0.0005 per retina, tsf = 1 per retina, and ΣQ^- = 13,899 ± 1,621 per retina [West et al., 1991; Bonthius et al., 2004]. We obtained pictures from 251 ± 1.20 grid sites per retina. The sampling frame within each grid was 50 × 50 μm, with an area of 0.0025 mm^2. We used the same counting frame across the whole retina following Hart [2001b], as we were interested in getting estimates of the relative densities of all photoreceptors. Pictures were taken and processed in a similar way as described above. Despite the care taken in the removal of the loosely attached pigmented epithelium, some of the tissue was too tightly adhered and therefore could not be removed without causing harm to the retina. To avoid bias in the counts, we did not consider those sites that contained damage (irregular distribution of oil droplets), that had photoreceptors which were folded over or bent, that had ablated oil droplets, or that had traces of pigmented epithelium. We acquired these photomicrographs using a ×40 objective lens under both bright and epifluorescent lights to distinguish the different oil droplets types (see below).

In birds, each type of oil droplet is associated with a specific type of photoreceptor [Bowmaker et al., 1997]. From microspectrophotometric analysis (see the next section), we identified 5 distinct types of oil droplets in the American goldfinch (T-type, C-type, Y-type, R-type, and P-type), which are associated with the following photoreceptor types: UVS single cone, short-wavelength-sensitive (SWS) single cone, medium-wavelength-sensitive (MWS) single cone, long-wavelength-sensitive (LWS) single cones, and the principal member of the double cone, respectively. Single cones are associated with chromatic vision, whereas double cones in birds have been associated with achromatic vision and

motion detection [von Campenhausen and Kirschfeld, 1998; Osorio et al., 1999; Goldsmith and Butler, 2005]. We followed the criteria of Hart [2001b] to distinguish the different oil droplet types (please see online suppl. appendix 2 for details).

We estimated the oil droplet density (number of droplets/mm^2) for each type of oil droplet (no tissue shrinkage correction was necessary because pictures were taken on fresh retinae). We also calculated the total number of different oil droplets (in single and double cones, and both types together), the SMO CE, and CE^2/CV^2 (table 1) based on the same equations used for retinal ganglion cells. All retinae had SMO CE values <0.1 and SMO CE^2/CV^2 ratios <0.5 (table 1), which indicates that our estimates were reliable. We built 6 topographic maps for each retina following the procedures described above [Stone, 1981; Ullmann et al., 2012], i.e. one for each type of photoreceptor and one considering all types of photoreceptors. In each retina, the proportional area of the range with the highest density (55,000–98,000 cells/mm^2) was calculated from the topographic map including all oil droplet types and then averaged. We used this average proportional area to determine the area of a concentric ring centered around the fovea. We then used the diameter of this ring to determine the width of 4 additional concentric rings. These rings were overlaid on each retina to plot the change in oil droplet densities across the retina.

Microspectrophotometry

A total of 11 goldfinches were used in microspectrophotometric analysis within 2–7 days of capture. Five individuals were in nonbreeding condition and 6 were in breeding condition. Prior to data collection, American goldfinches were light deprived (2–10 h) to enhance the regeneration of visual pigments. After extraction, we measured the eye axial length with a digital caliper and processed one eye immediately (alternating right and left eyes between individuals) and placed the other eye in a vial with PBS in ice shielded from light in the fridge to reduce tissue degradation for later processing. We then hemisected the eye just posterior to the lens at the ora serrata using a razor blade and removed the vitreous humor with tweezers and spring scissors. The retina was gently removed from the sclera and pigmented epithelium using a small paintbrush. We detached an approximately 6-mm^2 piece of retina and placed it on a Corning No. 1 glass slide (22 × 30 mm) where we macerated it using two razor blades. A drop of PBS and a drop of sucrose water were added to the macerated retina, which was covered with a Corning No. 1 coverslip (18 mm^2) and then sealed with black nail lacquer to prevent desiccation. Tissue processing and microspectrophotometric measurements were performed under infrared or dim red lights.

With a custom-made microspectrophotometer [MSP; Ellis Loew, Cornell University, Ithaca, N.Y., USA; design described in McFarland and Loew, 1994], we measured the absorbance [the amount of light absorbed as light passes through a substance; Liebman, 1972] of the cone and rod visual pigments in the outer segments, and the oil droplets in the inner segments. A Zeiss Ultrafluar Glyc objective (×32, NA 0.4) functioned as the condenser and a dry objective (×80, NA 0.9) functioned as the objective. An EX-Vision Super Circuits CCD camera attached to an 8-in TFT color LCD monitor covered in red Plexiglas was used to view the cell components. We isolated an area where there were individual photoreceptors and then took a baseline measurement in an empty area near the cells. Once we had obtained a baseline measurement, we made a scan of an isolated outer segment of a cone or rod, or individual oil droplet, in 1-nm increments from 350 to 750 nm. After this measurement, we placed a beam of white light on a target visual pigment for a minimum of 60 s to bleach the pigment and confirm its identity. Bleaching is necessary so that visual photopigments, which degrade in white light, can be distinguished from other nondegrading photoreactive substances present in the preparation [Liebman, 1972]. We only used for the analysis spectra where bleaching of the pigment occurred. We were also able to distinguish between MWS single cones and rods based on the shape of the outer segments [MWS single cones have smaller triangular shaped outer segments and rods have larger rectangular shaped ones with noticeable horizontal striations; Crescitelli, 1972] as these photoreceptors have absorbance curves that may overlap. Oil droplets are very conspicuous organelles, so no bleaching was necessary.

To determine the wavelength-specific peak sensitivity of the visual pigments (λ_{max}), we normalized individual absorbance spectra and fitted them to A1-rhodopsin templates using the MSP Control and Analysis Program [Loew and Stauble, 1988–1992]. Characterization of oil droplet absorbance spectra involves the determination of the wavelength at which a particular amount of light is absorbed. The three most widely used parameters are: λ_{cut}, the wavelength at which all light is absorbed by the oil droplet; λ_{mid}, the wavelength at which half of the light is absorbed, and λ_0, the wavelength at which 63% of light is absorbed (or the wavelength at which the transmittance equals 1/e) [Lipetz, 1984; Hart and Vorobyev, 2005]. Oil droplet λ values were determined from each spectrum using Microsoft Excel©.

During the sensitivity analysis, we normalized the region in the spectrum with rapidly increasing absorbance containing the λ parameters (long-wavelength arm of the absorbance curve) of each oil droplet spectra to one. To that end, we set the base of the long-wavelength arm to zero and then divided the spectra by the absorbance at the apex of the oil droplet long-wavelength arm. We then determined the wavelength at which the absorbance was 0.5 (λ_{mid}). After the λ_{mid} determination, we fitted a trend line to the region of the long-wavelength arm 10 nm on either side of the λ_{mid} parameter and recorded the slope, intercept, and R^2 parameters. Using the linear equation (absorbance = intercept + slope × wavelength) from the trend line, we calculated λ_{cut} by setting the absorbance to a value of one. Because λ_0 is a property of an oil droplet transmittance and not its absorbance, we calculated λ_0 mathematically as in Moore et al. [2012]. We graphed the absorbance curves of each visual pigment and oil droplet type by averaging the nonnormalized raw absorbance spectra within each visual pigment and oil droplet type. We then normalized each average spectrum to one as in Beason and Loew [2008]. Breeding and nonbreeding individuals were analyzed separately, but no differences were found so we pooled together all of the data to characterize goldfinch spectral sensitivity.

Statistical Analysis

We compared body mass and eye axial length between male and female goldfinches with general linear models. We also assessed the differences in the density of single and double cones between the dorsal and ventral parts of the retina by means of general linear models that accounted for the identity of each individual bird using a repeated measures design. We present means ± SE throughout.

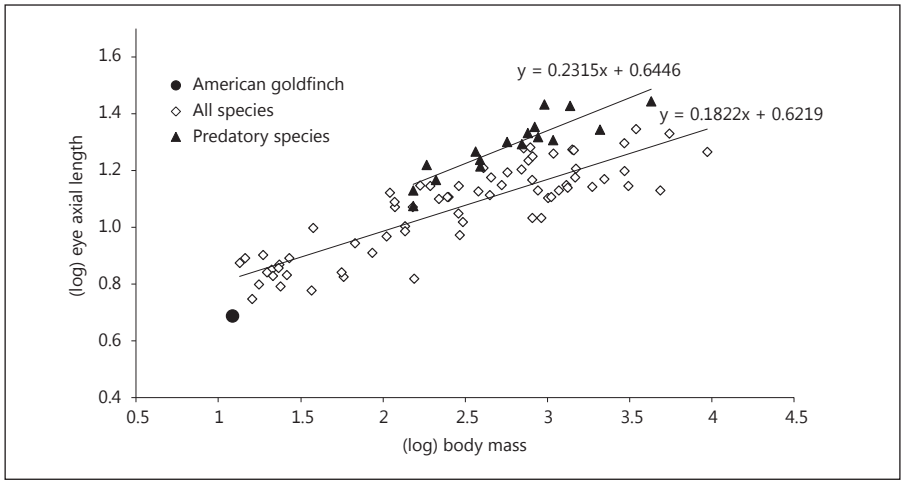

Fig. 1. Relationship between (log) eye axial length and (log) body mass. Data on 87 species with information on both parameters were obtained from Hall and Heesy [2011]. Plotted are the relationships for all 87 species from 25 families of Passeriformes and non-Passeriformes (diamonds) and for 17 predatory species belonging to the Falconidae and Accipitridae families (triangles). The American goldfinch is marked with a circle.

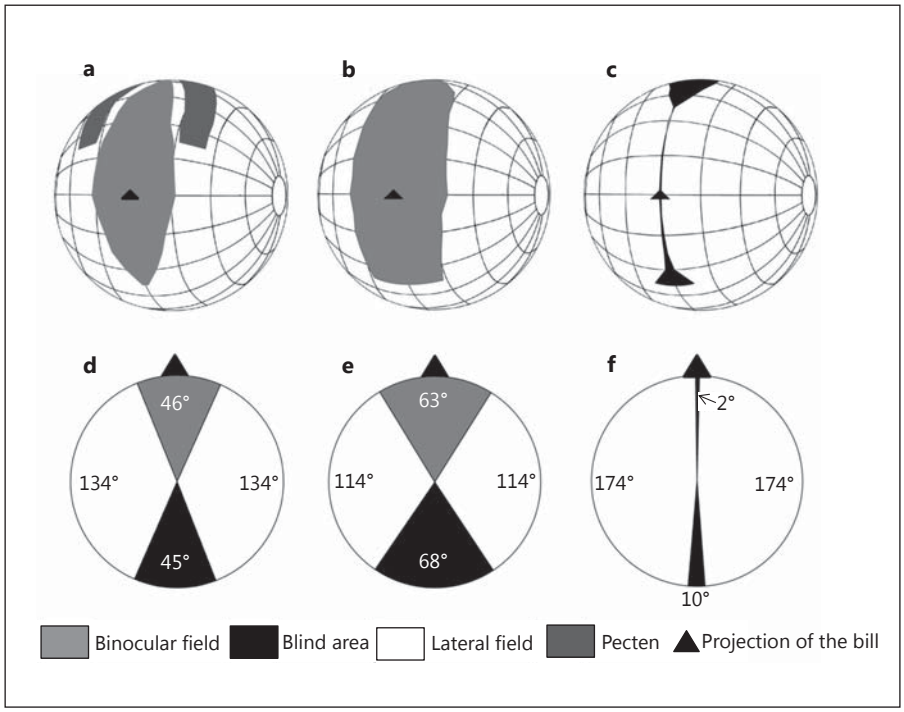

Fig. 2. Visual fields of the American goldfinch with eyes at rest (**a**, **d**), eyes converged (**b**, **e**), and eyes diverged (**c**, **f**). **a–c** Spherical projections of the boundaries of the visual fields of both eyes as well as the projection of the pecten in **a**. Lines represent a latitude and longitude coordinate system, with the equator vertically centered on the median sagittal plane, in increments of approximately 20°. The head of the bird is projected in the center of the sphere. The values used are averages from 8 individuals. **d–f** Horizontal slices showing the configuration of the visual fields on the horizontal plane (approximate plane of the bill).

Results

Eye Size

We measured both the eye axial length and the body mass of 12 of the studied individuals (6 males, 5 females, and 1 of unknown sex). Pooling all individuals, the mean eye axial length (averaged between the right and left eyes for each individual) was 4.88 ± 0.09 mm, and the body mass was 12.15 ± 0.29 g. There were no significant differences in eye axial length ($F_{1,9} = 0.01$, $p = 0.909$) or body mass ($F_{1,9} = 0.99$, $p = 0.344$) between males and females.

Considering data from Hall and Heesy [2011] on the relationship between eye axial length and body mass in 87 species (10 orders) of birds, we found that the relative size of the American goldfinch eye was slightly smaller than that expected for birds in general, and substantially smaller than that expected for predatory species from the families Falconidae and Accipitridae (fig. 1). One potential caveat of this analysis is the fact that most of the species in Hall and Heesy [2011] had body masses larger than the American goldfinch; therefore, adding smaller species to this relationship might change the results.

Visual Field Configuration

The bill of the goldfinch projects into the center of the binocular field on the horizontal plane (90–270°; fig. 2a–c), yet our measurements indicated that individuals were not able to see their bill tips. The width of the binocular field on the horizontal plane was 46° at rest (fig. 2d). Across all elevations, the average width of the binocular field was 26.64 ± 3.59° when the eyes were at rest, extending from 140° (below the bill) vertically to 0° (top of the head). The width of the blind area on the horizontal plane was 45°, with the maximum width of the blind area (50°) at 260° (fig. 2d, 3a). Across all elevations, the average width of the blind area was 32.94 ± 4.27° when the eyes were at rest, extending from 350° (just posterior to the top of the head) vertically to 260° (below the back of the head) (fig. 3a). The size of the lateral field on the horizontal plane was 134° at rest (fig. 2d), with the cyclopean visual field (= binocular + lateral right + lateral left visual fields) extending 315°. The average width of the pecten was 14.40 ± 0.48° when the eyes were at rest, extending from 60° (above the bill) vertically to 0° (top of the head).

American goldfinches showed a relatively high degree of eye movement. The largest eye movement amplitude (66°) was recorded on the horizontal plane (90–270°; fig. 3b). Across all elevations, the average degree of eye movement was 52.53 ± 1.48. The width of the binocular field increased by 17° from 46° at rest to 63° when the eyes converged (fig. 2e). Also, the width of the blind area increased by 23° from 45° at rest to 68° when the eyes converged (fig. 2e). The convergence of the eyes resulted in a reduction of the cyclopean visual field from 315 to 292° on the horizontal plane. When the eyes were fully diverged, the binocular field on the horizontal plane was abolished, resulting in a 2° blind area in front of the bill. As a result, the width of the blind area on the horizontal plane decreased from 45° at rest to 10° when the eyes diverged (fig. 2f). Eye divergence resulted in an increase in the cyclopean visual field from 315 to 358° on the horizontal plane.

Retinal Ganglion Cell Density and Distribution

We extracted 6 eyes from 3 individuals (axial length 4.74 ± 0.08 mm) and successfully processed 2 left retinae and 1 right retina. The density of the retinal ganglion cells was determined from 375.3 ± 8.8 frames from which cells could be identified. The overall mean density of retinal ganglion cells across the retina was 16,574 ± 1,478 cells/mm^2, with a mean peak density of 38,526 ± 5,201 cells/mm^2 (around the foveal area). The total number of cells per retina was estimated to be 810,127 ± 32,910 cells. Based on eye size and peak retinal ganglion cell densities, we estimated the visual acuity to be 5.40 cycles/degree.

Topographic maps created from these retinae show a concentric increase in retinal ganglion cell density from the retinal periphery (0–9,999 cells/mm^2) to the center of the retina (≥35,000 cells/mm^2; fig. 4a). We identified a potential fovea based on the presence of a pit on the wholemount, and we confirmed its presence via histological cross-sectioning (fig. 4b). The fovea was located almost centrally but was shifted towards the dorsal (0.52 mm from the center) and temporal (0.33 mm from the center) sides of the retina (fig. 4a). Based on the position of the orbits in the skulls, this dorsotemporal fovea would project slightly toward the frontal part of the skull (closer to the limit between the lateral and binocular fields) rather than directly sideways, and towards the edges of the binocular field (fig. 4c).

Photoreceptor Density and Distribution

Three left and 3 right eyes from 6 individuals (3 males, 3 females) were successfully processed (axial length 4.85 ± 0.05 mm). The density of oil droplets was determined from 161.8 ± 11.9 frames per retina from which oil droplets could be identified. The overall mean density of all oil droplet types across the retinae of the 6 individuals was 32,223 ± 2,197 per mm^2, with a mean peak density of 88,133 ± 3,338 per mm^2. The mean density of all single-cone photoreceptors combined (T-, C-, Y-, and R-type oil droplets, involved in chromatic vision) was 18,266 ± 787 per mm^2, and that of double-cone photoreceptors (P-type oil droplet, involved in achromatic vision and motion detection) was 13,957 ± 1,654 per mm^2. The mean densities of the different types of single cones were: UVS cone (T-type oil droplet), 2,442 ± 187 per mm^2; SWS cone (C-type oil droplet), 5,314 ± 361 per mm^2; MWS cone (Y-type oil droplet), 5,761 ± 343 per mm^2, and LWS cone (R-type oil droplet), 4,748 ± 347 per mm^2. Additionally, the total number of cone photoreceptors per retina was estimated to be 1,358,132 ± 153,221 (single cones, 693,197 ± 78,846; double cones, 1,017,691 ± 270,269).

Topographic maps show a concentric increase in the density of all photoreceptor types from the retinal periphery to the centrotemporal part of the retina (fig. 5, 6), which coincides approximately with the centrotemporal position of the fovea determined at the retinal ganglion cell layer (4a).

We divided the retina into dorsal and ventral parts via a line going through the center and assessed whether the combined density of single-cone photoreceptors and double-cones photoreceptors varied between the dorsal and ventral parts of the retina. The combined density of

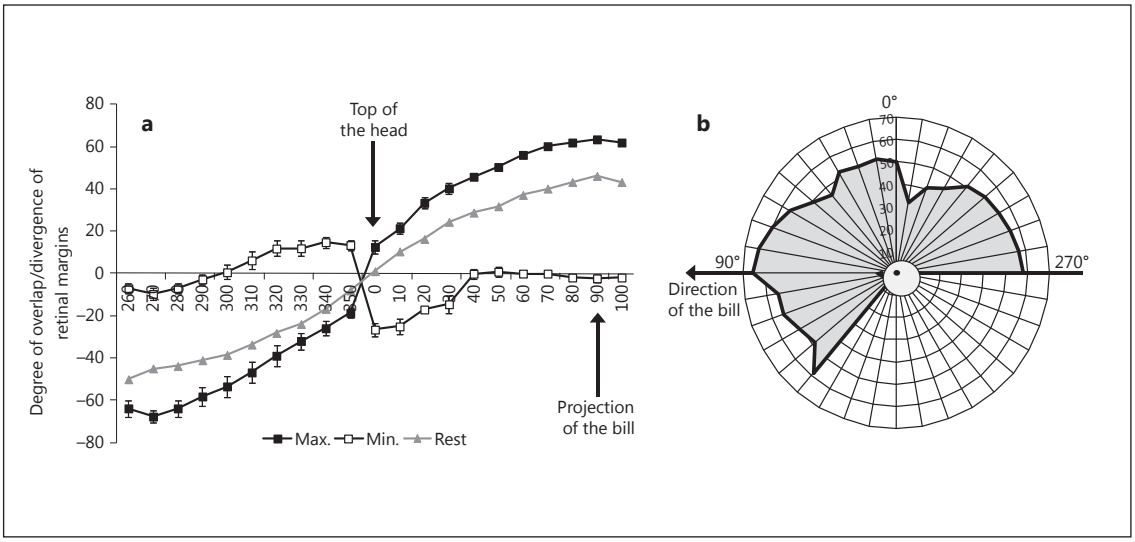

Fig. 3. a Mean (±SE) degree of overlap and divergence of retinal margins in the American goldfinch across different elevations along the median sagittal plane around the head with eyes at rest (triangles), eyes converged (black squares), and eyes diverged (white squares). Positive values represent binocular overlap, and negative values represent no visual coverage (blind area). **b** Average degree of eye movement along the median sagittal plane. The goldfinch head is included for ease of viewing, with the bill at 90°, the top of the head at 0°, and the back of the head 270°.

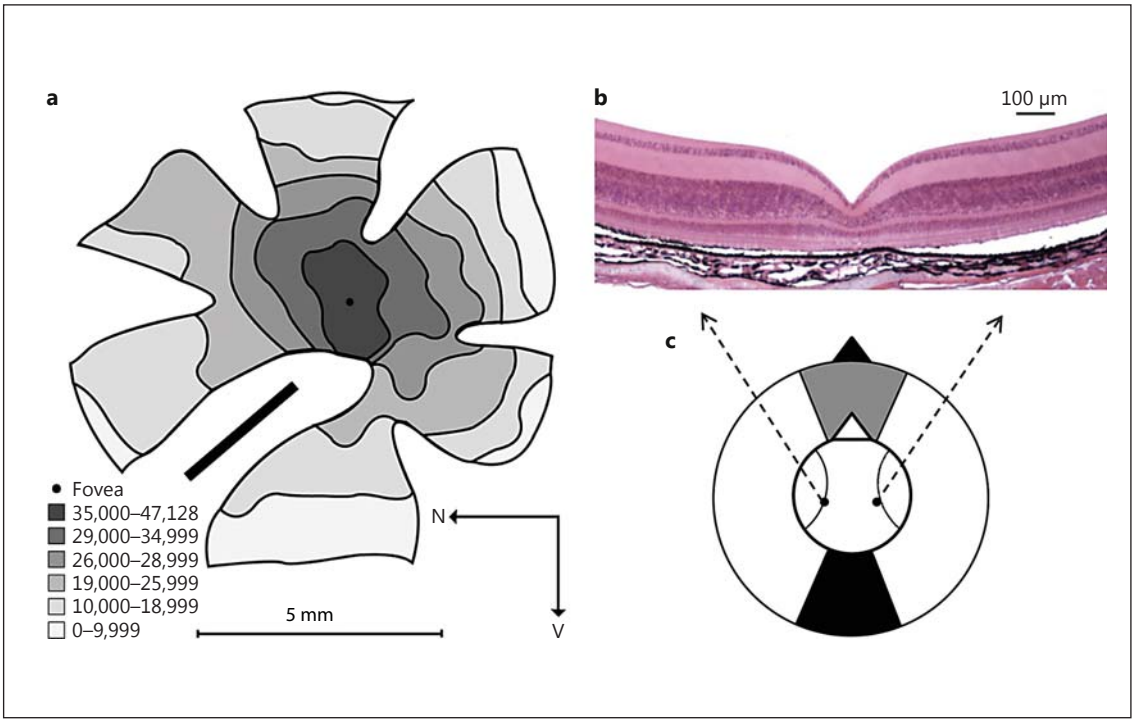

Color version available online

Fig. 4. a Isodensity topographic map representing the distribution of retinal ganglion cells in the ganglion layer of the American goldfinch retina. Ranges represent the number of retinal ganglion cells (in cells/mm^2). Presence of the fovea and pecten is indicated by the black dot and bar, respectively. N = Nasal; V = ventral. **b** Cross section of the goldfinch retinal tissue showing the foveal pit. **c** Top-view representation of the approximate projection of the fovea in the visual field of the American goldfinch with the eyes at rest.

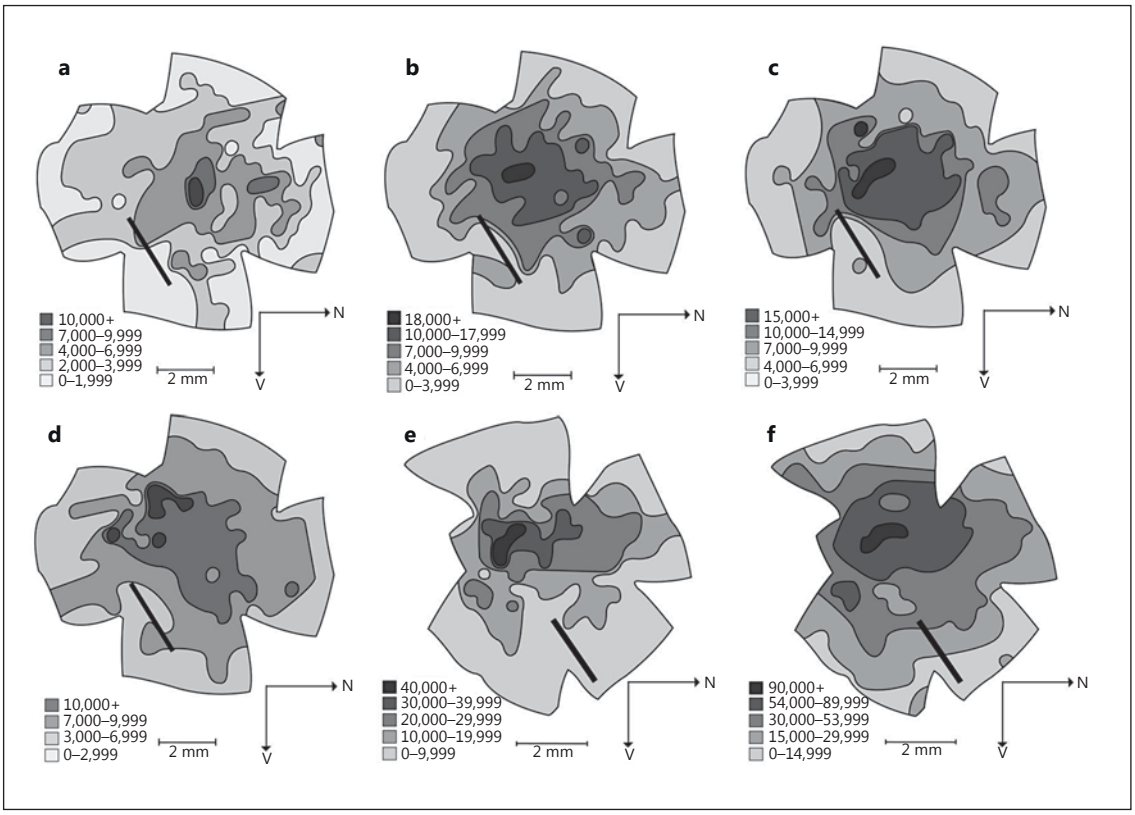

Fig. 5. Isodensity topographic maps representing the distribution of oil droplets by type in the American goldfinch photoreceptor layer. **a** T-type oil droplet in a UVS single cone. **b** C-type oil droplet in an SWS single cone. **c** Y-type oil droplet in an MWS single cone. **d** R-type oil droplet in an LWS single cone. **e** P-type oil droplet in a double cone. **f** All oil droplet types pooled together. Ranges represent the number of oil droplets (in cells/mm^2). Presence of the pecten is indicated by the black bars. N = Nasal; V = ventral.

single-cone photoreceptors was significantly higher in the dorsal part than in the ventral part of the retina ($F_{1,5} = 34.63$, $p = 0.002$; dorsal, 20,520 ± 510 oil droplets/mm^2; ventral, 16,213 ± 525 oil droplets/mm^2). There was no significant difference in the density of double-cone photoreceptors between the dorsal and ventral regions of the retina ($F_{1,5} = 0.01$, $p = 0.939$; dorsal, 11,484 ± 434 oil droplets/mm^2; ventral, 14,434 ± 448 oil droplets/mm^2).

Microspectrophotometry

We obtained data on visual pigment absorbance from 83 cones and 29 rods belonging to 11 birds (5 in nonbreeding condition and 6 in breeding condition). From the 5 nonbreeding birds, we collected data on visual pigment absorbance from 42 cones and 20 rods (table 2; 2 males, 3 females). From the 6 breeding birds, we collected data on visual pigment absorbance from 37 cones and 9 rods (3 males, 3 females). All single cones contained an A1-rhodopsin-shaped visual pigment as identified by template fitting (see Methods). Based on microspectrophotometry, we confirmed the presence of 4 distinct classes of single-cone photoreceptors and 1 class of double cone [fig. 7a–f; Hart, 2001a]. The nomenclature classification of the UVS and SWS peak absorbance followed Hart [2002] due to the lack of genetic data available to discriminate between the SWS1 and SWS2 pigments.

The peak absorbances (λ_{max}) of the 5 cone visual pigments were: 399 nm (UVS/VS single cone), 442 nm (SWS single cone), 512 nm (MWS single cone), 580 nm (LWS single cone), and 589 nm (double cone) (table 2; fig. 7). The peak absorbance of the rod visual pigment (RH1) was 515 nm (table 2), and it was distinguished from the MWS single cone based on cell shape. The principle double-cone visual pigment was distinguished from other LWS type pigments by its attachment to a P-type oil droplet. This criterion considerably decreased the sample size of double cones available, which in turn increased the noise of the normalized curves (fig. 7f).

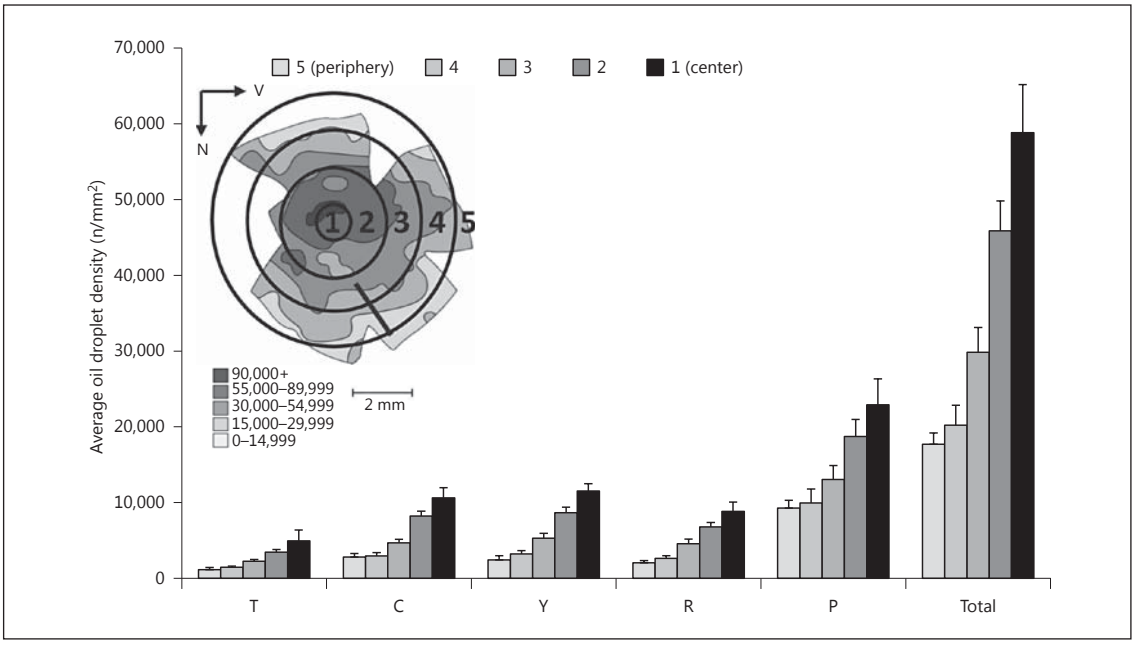

Fig. 6. Variations in oil droplet density across the retina. The bars represent the average density of oil droplets (n/mm^2) in each concentric ring; 1 = center of the retina (centered on the fovea that was determined by assessing the retinal ganglion cell layer) and radiating out concentrically to ring 5 = outermost edge of the retina. T = T-type oil droplet; C = C-type oil droplet; Y = Y-type oil droplet; R = R-type oil droplet; P = P-type oil droplet; Total = all oil droplet types combined.

Table 2. Mean ± SE of λ_{max} values, and n for 4 classes of single cones, 1 class of double cone, and 1 class of rod photoreceptor of the American goldfinch

	Rod	UVS/VS	Single cones			Double cone
			SWS	MWS	LWS	
Visual pigments						
Mean λ_{max} of the spectra, nm	515±1.3	399±2.7	442±2.1	512±1.1	580±1.3	589±7.0
Outer segments, n	29	7	9	30	25	3

	T-type	C-type	Y-type	R-type	P1-type	P2-type		P3-type
						a	b	
Oil droplets								
Mean λ_{mid}, nm		432±0.8	537±1.0	596±0.6	452±0.8	458±1.1	506±0.8	507±1.4
Mean λ_{cut}, nm		417±1.3	523±1.3	579±0.5	433±1.6	441±2.5	493±0.9	496±1.1
Mean λ_0, nm		428±0.9	533±1.1	592±0.6	447±0.9	453±1.37	503±0.8	505±1.3
Mean *b*		0.108±0.005	0.11±0.004	0.088±0.002	0.084±0.004	0.102±0.009	0.118±0.004	0.133±0.006
Mean B_{mid}		0.038±0.002	0.038±0.002	0.031±0.001	0.029±0.001	0.035±0.003	0.041±0.001	0.046±0.002
λ_{mid} of the mean absorbance spectrum, nm		434	536	594	452	458	506	508
λ_{cut} of the mean absorbance spectrum, nm		422	524	580	436	448	494	497
λ_0 of the mean absorbance spectrum, nm		431	533	590	448	455	503	505
b of the mean absorbance spectrum		0.120	0.120	0.104	0.092	0.147	0.042	0.127
B_{mid} of the mean absorbance spectrum		0.041	0.041	0.036	0.032	0.051	0.042	0.044
Oil droplets, n	6	53	27	64	50	19		20

Mean ± SE of λ_{mid}, λ_{cut}, λ_0, *b*, B_{mid} values, and n for the individual oil droplet spectra associated with visual pigments and the averaged spectrum for each type.

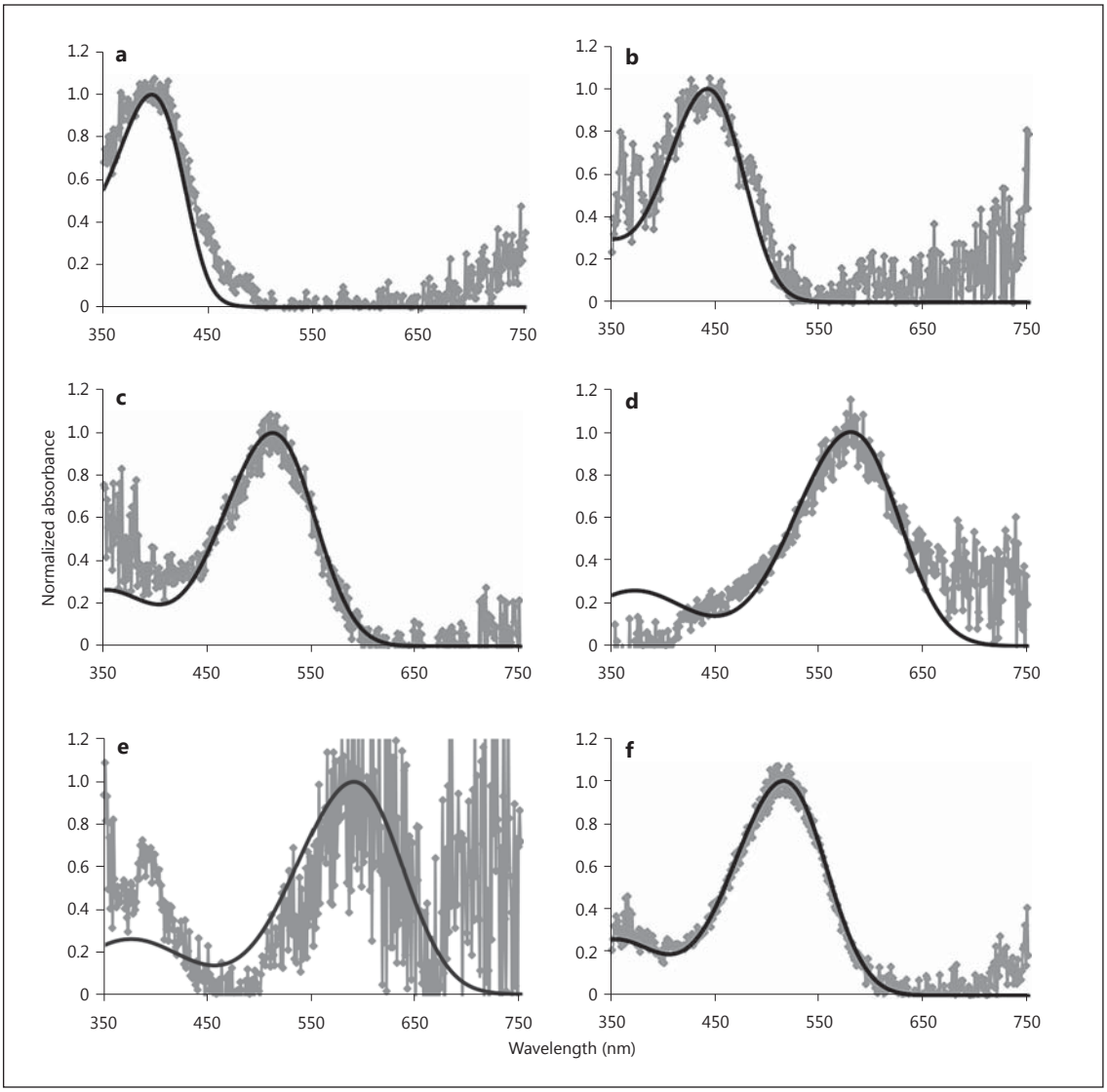

Fig. 7. Normalized absorbance spectra of the American goldfinch photoreceptors. **a** UVS/VS cone. **b** SWS cone. **c** MWS cone. **d** LWS cone. **e** Double cone. **f** Rod (RH1). **a–f** The solid black line is an A1-rhodopsin pigment template from Govardovskii et al. [2000].

We identified 5 oil droplet types from 252 oil droplets measured from 11 birds (5 in nonbreeding condition, 6 in breeding condition): T-type, C-type, P-type, Y-type, and R-type. Spectra were classified following previous studies [Bowmaker et al., 1997; Hart, 2001a]. We segregated the P-type oil droplets into 3 variants, i.e. P1, P2, and P3, based on the shape of the spectra, to show the variation that occurs in the absorbance of the principal member oil droplets as a result of differences in carotenoid content [Hart, 2001b; Knott, 2010, 2012]. The P2 variant contained 2 peaks hereafter referred to as P2 (a), or the higher absorbance peak, and P2 (b), or the lower absorbance peak. We confirmed that the principal and accessory members contained the same P-type oil droplet by measuring a double cone with both oil droplets that remained attached to the inner segment of the photoreceptor.

Table 2 presents the λ_{cut}, λ_{mid}, and λ_0 values of oil droplets by pooling data from breeding and nonbreeding individuals (fig. 8a, b). The T type oil droplet is transparent due to a lack of carotenoids [Hart, 2001a]; therefore, the absorbance parameters could not be measured.

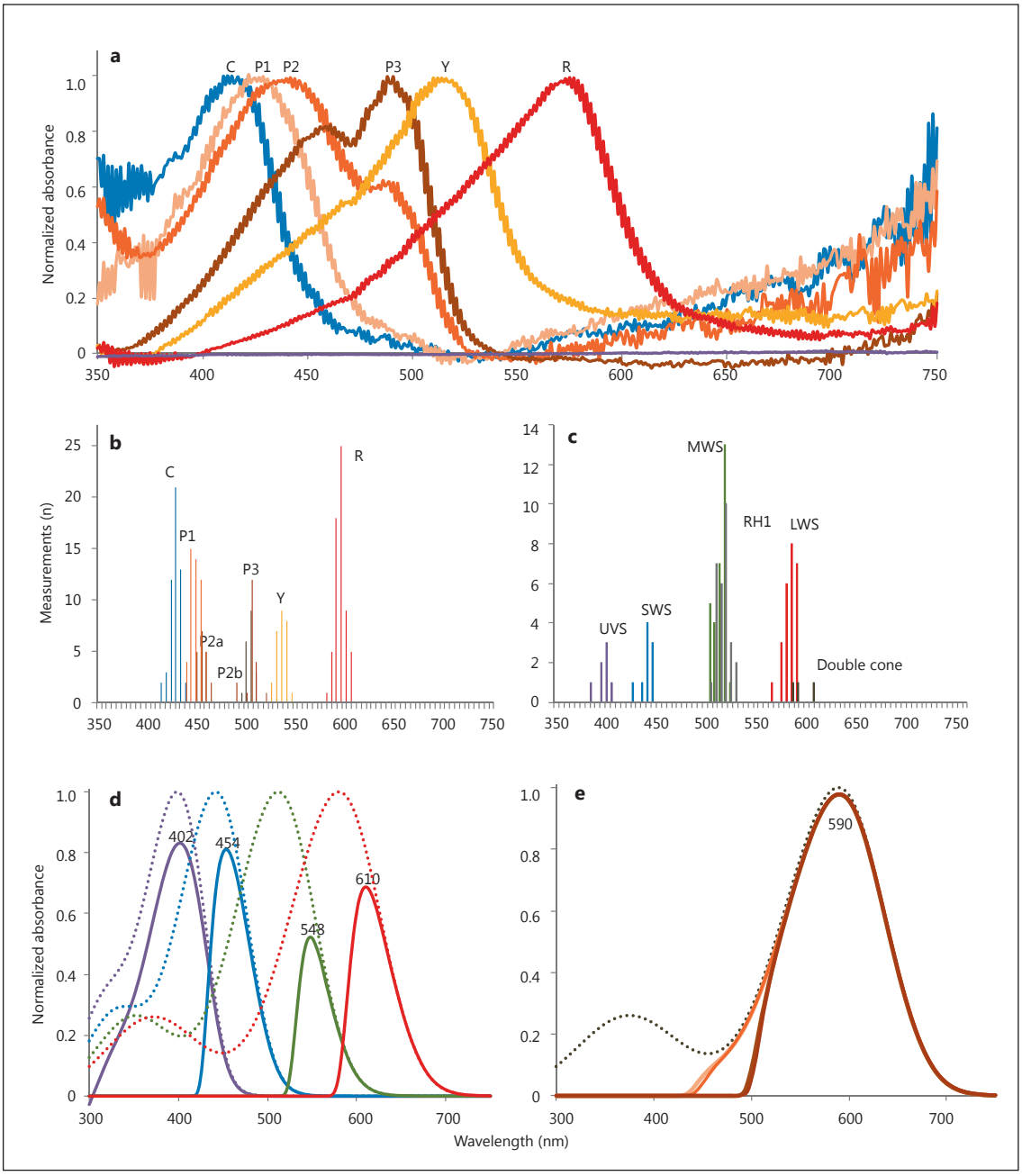

Color version available online

Fig. 8. Normalized absorbance spectra of the American goldfinch oil droplets. **a** From left to right: C-type oil droplet (blue in the online version/black in the printed version), P1-type oil droplet (peach/charcoal grey), P2-type oil droplet (orange/dark grey), P3-type oil droplet (dark orange/grey), Y-type oil droplet (yellow/light grey), R-type oil droplet (red/smokey grey), and T-type oil droplet (purple; not normalized to 1 in this figure for ease of viewing). **b** Histogram of λ_{mid} values for each oil droplet type [C-type, P1-type, P2a-type (orange/light grey), P2b-type (dark orange/grey), P3-type (red-orange), Y-type, and R-type] that were used to calculate the mean oil droplet spectra in **a**. **c** Histogram of λ_{max} values for each visual pigment type [UVS/VS (purple/black), SWS (blue/black), MWS (green/black), RH1 (grey/light grey), LWS (red/black), and double cone (dark brown/grey)] that were used to calculate the mean visual pigment spectra (fig. 7a–e). **d** Absorbance spectra of the 4 classes of single cones. Solid lines from left to right: UVS/VS (402 nm), SWS (454 nm), MWS (548 nm), LWS (610 nm). **e** Absorbance spectra of the double cone. Solid lines from left to right: P1-type (peach/black), P2-type (P2a: orange/light grey; P2b: dark orange/grey), P3-type (red-orange/dark grey). In **d** and **e**, dotted lines represent the visual pigment curves from figure 7a–e created from Govardovskii et al. [2000], and solid lines represent the sensitivity of the overall photoreceptor considering the effects of the transmittance of the ocular media and oil droplets and the absorbance of the visual pigments.

We calculated the overall cone sensitivity by considering the transmittance of the oil droplets and the absorbance of the visual pigments in the American goldfinch [Govardovskii et al., 2000; Hart and Vorobyev, 2005]. We produced an ocular media transmittance curve following Endler and Mielke [2005]. As a result, the overall peak sensitivities of the single and double cones shifted to longer wavelengths than those of the visual pigment they contained (fig. 8d, e). The sensitivities of the single cones were determined as: 402 nm (UVS), 454 nm (SWS), 548 nm (MWS), and 610 nm (LWS) (fig. 8d). The sensitivity of the double cone was determined as 590 nm for all three P-type oil droplets (fig. 8e). These values should be interpreted with care because we could not measure the ocular media transmission curve for American goldfinches.

Discussion

Our results show that American goldfinches have many features characteristic of the visual traits of species that feed on passive prey (i.e. relatively small eyes, wide lateral fields via divergent eye movements, a single fovea), but, contrary to our expectations, they also have some visual traits which are more characteristic of predatory species (e.g. foveae projecting towards the frontal part of the skull via convergent eye movements).

In terms of overall visual resolution (determined mostly by eye size), American goldfinches fit the profile of species that do not seek active prey given their relatively small eyes in relation to their body mass compared to predatory species and also to other birds in general (fig. 1). The implication is that goldfinches would have a relatively lower probability of detecting visual stimuli (e.g. predators) from far distances [Tisdale and Fernández-Juricic, 2009]. However, American goldfinches have relatively high peak retinal ganglion cell densities (38,526 cells/mm^2) compared to some of the other Passeriformes studied to date [tree sparrow, 26,000 cells/mm^2, Rahman et al., 2007; brown-eared bulbul, 24,032 cells/mm^2, Rahman et al., 2008; house finch, 25,256 cells/mm^2, house sparrow, 23,920 cells/mm^2, brown-headed cowbird, 21,665 cells/mm^2, European starling, 25,317 cells/mm^2, Dolan and Fernández-Juricic, 2010; white-breasted nuthatch, 35,850 cells/mm^2, tufted titmouse, 35,850 cells/mm^2, Carolina chickadee, 28,969 cells/mm^2, Moore et al., 2013], although the densities are lower than in other species [great kiskadee, 55,000 cells/mm^2, rusty-marginated flycatcher, 65,000 cells/mm^2, yellow-bellied eleania and mouse-colored tyrannulet, ~150,000 cells/mm^2; Coimbra et al., 2006, 2009]. Differences in peak densities may be related to methodological differences between studies; for instance, Coimbra et al. [2006, 2009] counted all neurons (both ganglion and amacrine cells), whereas our study only focused on retinal ganglion cells. Despite these differences, it seems that goldfinches may compensate for their relatively low overall spatial resolution by increasing their localized spatial resolution [see also Dolan and Fernández-Juricic, 2010]. This would enhance the relative sensory value of the goldfinch fovea as the source of high quality (e.g. high-resolution) information given its relatively small retina.

American goldfinches actually have wider binocular fields than some avian diurnal predators [hawks and eagles, 33–40°; Martin and Katzir, 1999; O'Rourke et al., 2010] and even some other Passeriformes [e.g. Fernández-Juricic et al., 2008, 2010]. Wide binocular fields have been implicated in activities that require precise manipulation of food items with the bill during foraging, particularly in species that can see their bill tips [Martin, 2009], although that is not the case in goldfinches. However, wide binocular fields may also facilitate searching for and detecting food items over a wider area through contrast discrimination [Blake et al., 1981]. Goldfinches often forage on the tips of stems or branches, including hanging upside down [McGraw and Middleton, 2009]. Successful seed extraction under these conditions may require careful assessment of the distance and relative position of the bill in relation to the foraging substrate; a process that may be facilitated by a wider overlap of the right and left visual fields.

One of the reasons behind the wider binocular fields of birds foraging on passive versus active prey may be related to their retinal configuration [Fernández-Juricic et al., 2011a]. In general, diurnal raptors have two foveae: one projecting laterally with a higher visual resolution to detect and track prey and one projecting binocularly with a lower visual resolution to catch and manipulate prey at close quarters [Reymond, 1985, 1987; Inunza et al., 1991; Tucker, 2000]. A similar retinal configuration with two retinal specializations (either two foveae or one fovea and one area) is present in other sit-and-wait avian foragers [Moroney and Pettigrew, 1987; Coimbra et al., 2006]. This dual-retinal specialization configuration partitions the detection and catching of prey in different parts of the visual field (lateral and binocular, respectively) and at different distances (far and close, respectively). On the other hand, we found that American goldfinches have a single fovea with high densities of both retinal ganglion cells and photoreceptors. The goldfinch fovea is centrotemporally

located and thus projects towards the frontal part of the skull. With the high degree of eye convergence, goldfinches may likely bring the foveae close to the edges of the binocular field, which would increase not only its width but also its visual resolution. A similar combination of fovea position and eye movements has been found in other Passeriformes that forage on the ground and seek a large proportion of passive prey [Fernández-Juricic et al., 2011b]. Consequently, this single-fovea configuration allocates both detection and grabbing of food items at close distances within the binocular field. The overall implication is that avian binocular vision may be configured differently in birds that seek passive versus active prey, which could partly explain the different trends in the width of the binocular field of these avian groups compared to their mammalian counterparts [Heesy and Hall, 2010].

The distribution of photoreceptors also revealed some interesting patterns. The American goldfinch fovea seems to be the center of both chromatic and achromatic/motion vision, as both single and double cones are more abundant around the foveal area. This sensory configuration may account for the high degree of eye movement of goldfinches, which would be necessary to move the single fovea around and improve the detection and tracking of visual stimuli. For instance, goldfinches are known for chewing seeds in head-up positions, allowing them to engage in vigilance behavior while foraging [Popp, 1988; Desportes et al., 1990]. During these food-handling bouts, goldfinches could increase the panoramic view around their heads by diverging their eyes, and reducing the size of the blind area to as little as 10°, which would increase the chances of detecting predators.

The density of double cones, associated with motion detection, did not vary between the dorsal and ventral parts of the retina, as found in avian ground foragers [Hart, 2001b], yet the density of single cones was significantly higher in the dorsal versus ventral parts of the retina. Consequently, chromatic vision is expected to be more acute towards the foraging substrate, due to the retinal curvature, when goldfinches are head-up handling seeds or hanging upside down exploring composite plants [McGraw and Middleton, 2009]. This photoreceptor distribution could enhance the discrimination of food items against the background through chromatic contrast. Similar higher densities of certain types of single cones have been found in other avian species with different foraging techniques [e.g. Goldsmith et al., 1984; Hart et al., 1998].

The retina of the American goldfinch contains 4 single cone types and 1 rod type. This is consistent with the avian tetrachromatic visual system [Bowmaker et al., 1997; Hart, 2001a]. We used the criterion of Hart [2001a] to classify the sensitivity of the visual pigment with the shortest wavelength sensitivity, in which a peak value <400 nm is considered to be UVS. Interestingly, the American goldfinch UVS cone peak sensitivity (399 nm) falls very close to the limit between UVS and VS sensitivity [Bowmaker et al., 1997; Hart and Hunt, 2007; Ödeen et al., 2011]. However, when considering the overall sensitivity of the UVS goldfinch photoreceptor, which factors in the ocular media, the peak sensitivity goes up to 402 nm, which falls within the VS sensitive classification range mentioned before. We did not measure the transmittance of the goldfinch ocular media but used the approximation proposed by Endler and Mielke [2005]. Therefore, we are uncertain as to how the ocular media could influence the 399-nm peak of the goldfinch photoreceptor.

The UVS peak sensitivity of the single cone in the American goldfinch is shifted 26 nm higher from the nearest UVS cone in passerines [373 nm in the white-headed munia *Lonchura maja*; Hart, 2001a], and 4 nm lower than the nearest VS cone [403 nm in the bobolink; Beason and Loew, 2008; Ödeen et al., 2009]. In general, the differences in peak sensitivity between these two variants (VS, 403–426 nm; UVS, 360–380 nm) may arise from amino acid substitutions in the opsin protein found in the SWS1 visual pigment [Ödeen and Håstad, 2003; Hart and Hunt, 2007; Ödeen et al., 2011]. For instance, the pigeon *Columba livia* has a UVS cone with a peak at 393 nm due to a substitution of 4 amino acids in the opsin gene sequence which causes a 19- to 33-nm shift in sensitivity from the 360- to 374-nm UVS range found in other species [Shi and Yokoyama, 2003].

Furthermore, the SWS2 pigment peak sensitivity (SWS cone) is thought to covary with that of the UVS and VS variants of the SWS1 pigment to minimize the loss of color discrimination [Ödeen and Håstad, 2003; Ödeen et al., 2011]. For instance, in species with a UVS cone, the peak sensitivity of the SWS cone is shifted towards shorter wavelengths [427–454 nm in Passeriformes; Hart and Hunt, 2007]. In species with a VS cone, the peak sensitivity of the SWS cone is shifted towards longer wavelengths [451–480 nm; Ödeen et al., 2011]. Accordingly, the fact that the peak sensitivity of the goldfinch SWS cone is 442 nm would support a UVS visual pigment in this species. The molecular characterization of this visual pigment, however, could help establish whether it is UVS or VS visual system.

From a functional perspective, seeing in the near-UV range of the spectrum may allow both male and female goldfinches to assess the UV reflectance from the yellow plumage of potential mates (peak UV reflectance ~370–380 nm), which has been associated with assortative mating [MacDougall and Montgomerie, 2003]. Furthermore, signaling and perceiving in the UV range of the spectrum may allow goldfinches to reduce the conspicuousness of their breeding plumage to the eyes of avian predators [Håstad et al., 2005], which generally have a VS visual system [Ödeen and Håstad, 2003]. Additionally, goldfinches forage on composite plants [McGraw and Middleton, 2009], whose flowers are known to reflect in the UV or near-UV [Chittka et al., 1994]. Therefore, the reflectance curves of these flowers would overlap with the sensitivities of both the UVS and the SWS goldfinch photoreceptors. By having two photoreceptors with sensitivities at this near-UV range of the spectrum, goldfinches may benefit by having enhanced color discrimination of food resources.

We also found differences in the peak sensitivity of the goldfinch RH1, MWS, and LWS photoreceptors compared to other bird species [Hart and Hunt, 2007], but to a lesser extent than that of the UVS cone. For instance, the goldfinch RH1 and MWS visual pigment peak sensitivities were 6 and 3 nm higher, respectively, than those of other bird species [RH1, 500–509 nm; MWS, 497–509 nm; Hart, 2001a; Hart and Hunt, 2007; Beason and Loew, 2008]. The LWS visual pigment peak sensitivity was 9 nm higher compared to other birds [543–571 nm; Hart, 2001a; Hart and Hunt, 2007], although LWS pigment has shown a high degree of between-species variability. However, when combining the effects of visual pigment sensitivity and the absorbance of the oil droplets associated with them, the overall sensitivities of all American goldfinch single-cone classes fall within the ranges reported previously in other species [Hart and Hunt, 2007]. Therefore, from a functional perspective (i.e. overall photoreceptor sensitivities), the differences in color perception between the goldfinch and other species may not be as pronounced, but future studies should test this through modeling (e.g. visual contrast) and empirical (e.g. behavioral) approaches.

The characterization of different visual dimensions in the American goldfinch provided a better understanding of the visual system of a bird species seeking passive prey. The general paradigm, deeply rooted in the mammalian sensory literature [Hughes, 1977; Cronin, 2005], is that passive and active prey foragers have different visual systems. However, the American goldfinch specifically showed traits of both, partially due to a flexible visual field configuration that allows individuals to quickly change the size of the binocular, lateral, and blind areas to adjust for food exploitation or predator detection. This is done by moving the fovea around through eye and head movements. Overall, the American goldfinch visual system seems quite specialized in detecting and handling passive food items at very close distances. More work is necessary at the comparative level to determine whether these sensory adaptations are more widespread in other Passeriformes or the goldfinch represents a special case.

Acknowledgements

We thank Jeff Lucas and Richard Howard for their comments on an earlier version of this paper. Central Garden and Pet Company and Purdue University provided funding for this study.

References

Beason RC, Loew ER (2008): Visual pigment and oil droplet characteristics of the bobolink *(Dolichonyx oryzivorus),* a new world migratory bird. Vision Res 48:1–8.

Blake R, Sloane M, Fox R (1981): Further developments in binocular summation. Perceptual Psychophysics 30:266–276.

Bonthius DJ, McKim R, Koele L, Harb H, Karacay B, Mahoney J, Pantazis NJ (2004): Use of frozen sections to determine neuronal number in the murine hippocampus and neocortex using the optical dissector and optical fractionator. Brain Res Brain Res Protoc 14:45–57.

Bowmaker JK (2008): Evolution of vertebrate visual pigments. Vision Res 48:2022–2041.

Bowmaker JK, Heath LA, Wilkie SE, Hunt DM (1997): Visual pigments and oil droplets from six classes of photoreceptor in the retinas of birds. Vision Res 37:2183–2194.

Chittka L, Shmida A, Troje N, Menzel R (1994): Ultraviolet as a component of flower reflections, and the colour perception of Hymenoptera. Vision Res 34:1489–1508.

Coimbra JP, Marceliano MLV, Andrade-da-Costa BLD, Yamada ES (2006): The retina of tyrant flycatchers: topographic organization of neuronal density and size in the ganglion cell layer of the great kiskadee *Pitangus sulphuratus* and the rusty margined flycatcher *Myiozetetes cayanensis* (Aves: *Tyrannidae*). Brain Behav Evol 68:15–25.

Coimbra JP, Trevia N, Marceliano ML, Da Silveira Andrade-Da-Costa LB, Picanco-Diniz CW, Sumi Yamada E (2009): Number and distribution of neurons in the retinal ganglion cell layer in relation to foraging behaviors of tyrant flycatchers. J Comp Neurol 514:66–73.

Crescitelli F (1972): The visual cells and visual pigments of the vertebrate eye. Handb Sens Physiol 2:245–363.

Cronin TW (2005): The visual ecology of predator-prey interactions; in Barbosa P, Castellanos I (eds): Ecology of Predator-Prey Interactions. Oxford, Oxford University Press, pp 105–138.
Cuthill IC (2006): Color perception; in Hill GE, McGraw KJ (eds): Bird Coloration: Mechanisms and Measurements. Cambridge, Harvard University Press, vol 1, pp 3–40.
Desportes JP, Metcalfe NB, Popp JW, Meyer RM, Gallo A, Cézilly F (1990): The predictability and patterns of vigilant behavior. Behav Processes 22:41–46.
Dolan T, Fernández-Juricic E (2010): Retinal ganglion cell topography of five species of ground foraging birds. Brain Behav Evol 75:111–121.
Ehrlich D (1981): Regional specialization of the chick retina as revealed by the size and density of neurons in the ganglion cell layer. J Comp Neurol 195:643–657.
Elphick C, Dunning JB Jr, Sibley DA (2001): The Sibley Guide to Bird Life and Behavior – National Audubon Society. New York, Knopf.
Endler JA, Mielke PW Jr (2005): Comparing entire colour patterns as birds see them. Biol J Linn Soc Lond 86:405–431.
Fernández-Juricic E, Gall MD, Dolan T, O'Rourke C, Thomas S, Lynch JR (2011a): Visual systems and vigilance behaviour of two ground-foraging avian prey species: white-crowned sparrows and California towhees. Anim Behav 81:705–713.
Fernández-Juricic E, Gall MD, Dolan T, Tisdale V, Martin GR (2008): The visual fields of two ground foraging birds, house finches and house sparrows, allow for simultaneous foraging and anti-predator vigilance. Ibis 150: 779–787.
Fernández-Juricic E, Moore BA, Doppler M, Freeman J, Blackwell BF, Lima SL, DeVault TL (2011b): Testing the terrain hypothesis: Canada geese see their world laterally and obliquely. Brain Behav and Evol 77:147–158.
Fernández-Juricic E, O'Rourke C, Pitlik T (2010): Visual coverage and scanning behavior in two corvid species: American crow and Western scrub jay. J Comp Physiol A Neuroethol Sens Neural Behav Physiol 196:879–888.
Freeman B, Tancred E (1978): The number and distribution of ganglion cells in the retina of the brush-tailed possum, *Trichosurus vulpecula*. J Comp Neurol 177:557–567.
Garamszegi LZ, Møller AP, Erritzøe J (2002): Coevolving avian eye size and brain size in relation to prey capture and nocturnality. Proc Biol Sci 269:961–967.
Glaser EM, Wilson PD (1998): The coefficient of error of optical fractionator population size estimates: a computer simulation comparing three estimators. J Microsc 192:163–171.
Goldsmith TH, Butler BK (2005): Color vision of the budgerigar *(Melopsittacus undulatus):* hue matches, tetrachromacy, and intensity discrimination. J Comp Physiol A Neuroethol Sens Neural Behav Physiol 191:933–951.
Goldsmith TH, Collins JS, Licht S (1984): The cone oil droplets of avian retinas. Vision Res 24:1661–1671.
Govardovskii VI, Fyhrquist N, Reuter T, Kuzmin DG, Donner K (2000): In search of the visual pigment template. Vis Neurosci 17:509–528.
Gundersen HJG (1977): Notes on the estimation of the numerical density of arbitrary profiles: the edge effect. J Microsc 111:219–223.
Hall MI, Heesy CP (2011): Eye size, flight speed and Leuckhart's law in birds. J Zool 283:291–297.
Hart NS (2001a): The visual ecology of avian photoreceptors. Prog Retin Eye Res 1:675–703.
Hart NS (2001b): Variations in cone photoreceptor abundance and the visual ecology of birds. J Comp Physiol A Neuroethol Sens Neural Behav Physiol 187:685–698.
Hart NS (2002): Vision in the peafowl (Aves: *Pavo cristatus*). J Exp Biol 205:3925–3935.
Hart NS, Hunt DM (2007): Avian visual pigments: characteristics, spectral tuning, and evolution. Am Nat 169:S7–S26.
Hart NS, Partridge JC, Cuthill IC (1998): Visual pigments, oil droplets and cone photoreceptor distribution in the European starling *(Sturnus vulgaris).* J Exp Biol 201:1433–1446.
Hart NS, Vorobyev M (2005): Modeling oil droplet absorption spectra and spectral sensitivities of bird cone photoreceptors. J Comp Physiol A Neuroethol Sens Neural Behav Physiol 191:381–392.
Håstad O, Victorsson J, Ödeen A (2005): Differences in color vision make passerines less conspicuous in the eyes of their predators. Proc Nat Acad Sci USA 102:6391–6394.
Heesy CP, Hall MI (2010): The nocturnal bottleneck and the evolution of mammalian vision. Brain Behav Evol 75:195–203.
Hughes A (1977): The topography of vision in mammals of contrasting life style: comparative optics and retinal organization; in Crescitelli F (ed): The Visual System in Vertebrates. New York, Springer, pp 615–756.
Inunza O, Bravo H, Smith R, Angel M (1991): Topography and morphology of retinal ganglion cells in Falconiforms: a study on predatory and carrion-eating birds. Anat Rec 229:271–277.
Kiltie RA (2000): Scaling of visual acuity with body size in mammals and birds. Funct Ecol 14:226–234.
Knott B, Berg ML, Morgan ER, Buchanan KL, Bowmaker JK, Bennett ATD (2010): Avian retinal oil droplets: dietary manipulation of colour vision? Proc Biol Sci 277:953–962.
Knott B, Bowmaker JK, Berg ML, Bennett ATD (2012): Absorbance of retinal oil droplets of the budgerigar: sex, spatial and plumage morph-related variation. J Comp Physiol A Neuroethol Sens Neural Behav Physiol 198: 43–51.
Liebman PA (1972): Microspectrophotometry of photoreceptors. Handb Sens Physiol 2:481–528.
Lipetz LE (1984): A new method for determining peak absorbance of dense pigment samples and its application to the cone oil droplets of *Emydoidea blandingii.* Vision Res 24:597–604.
Lisney TJ, Collin SP (2007): Relative eye size in elasmobranchs. Brain Behav Evol 69:266–279.
Lisney TJ, Iwaniuk AN, Bandet MV, Wylie DR (2012): Eye shape and retinal topography in owls (Aves: *Strigiformes*). Brain Behav Evol 79:218–236.
Lisney TJ, Stecyk K, Kolominsky J, Schmidt BK, Corfield JR, Iwaniuk AN, Wylie DR (2013): Ecomorphology of eye shape and retinal topography in waterfowl (Aves: Anseriformes: Anatidae) with different foraging modes. J Comp Physiol A Neuroethol Sens Neural Behav Physiol 199:385–402.
Loew ER, Stauble M (1988–1992): MSP Control and Analysis Program (computer software). Ithaca, New York State College of Veterinary Medicine.
MacDougall AK, Montgomerie R (2003): Assortative mating by carotenoid-based plumage colour: a quality indicator in American goldfinches, *Carduelis tristis.* Naturwissenschaften 90:464–467.
Martin GR (1984): The visual fields of the tawny owl, *Strix aluco* L. Vision Res 24:1739–1751.
Martin GR (1986): The eye of a passeriform bird, the European starling *(Sturnus vulgaris):* eye movement amplitude, visual fields and schematic optics. J Comp Physiol A Neuroethol Sens Neural Behav Physiol 159:545–557.
Martin GR (1993): Producing the image; in Zeigler HP, Bischof H-J (eds): Vision, brain and behaviour in birds. Massachusetts, MIT Press, pp 5–24.
Martin GR (2007): Visual fields and their functions in birds. J Ornithol 148:S547–S562.
Martin GR (2009): What is binocular vision for? A birds' eye view. J Vision 9:1–19.
Martin GR, Katzir G (1999): Visual field in short-toed eagles *Circaetus gallicus* and the function of binocularity in birds. Brain Behav Evol 53: 55–66.
McFarland WN, Loew ER (1994): Ultraviolet visual pigments in marine fishes of the family *Pomacentridae.* Vision Res 34:1393–1396.
McGraw KJ, Middleton AL (2009): American goldfinch *(Spinus tristis);* in Poole A (ed): The Birds of North America Online. Ithaca, Cornell Lab of Ornithology. http://bna.birds.cornell.edu/bna/species/080.
McIlwain JT (1996): An Introduction to the Biology of Vision. Cambridge, Cambridge University Press.
Meyer DBC (1977): The avian eye and its adaptations; in Crescitelli F (ed): The Visual System of Vertebrates: Handbook of Sensory Physiology. New York, Springer, vol VII(5), pp 549–612.
Moore BA, Baumhardt P, Doppler M, Randolet J, Blackwell BF, DeVault TL, Loew ER, Fernández-Juricic E (2012): Oblique color vision in an open-habitat bird: spectral sensitivity, photoreceptor distribution and behavioral implications. J Exp Biol 215:3442–3452.

Moore BA, Doppler M, Young JE, Fernandez-Juricic E (2013): Interspecific differences in the visual system and scanning behavior of three forest passerines that form heterospecific flocks. J Comp Physiol A Neuroethol Sens Neural Behav Physiol 199:263–277.

Moroney MK, Pettigrew JD (1987): Some observations on the visual optics of kingfishers *(Aves*, *Coraciformes*, *Alcedinidae).* J Comp Physiol A Neuroethol Sens Neural Behav Physiol 160:137–149.

Ödeen A, Hart NS, Håstad O (2009): Assessing the use of genomic DNA as a predictor of the maximum absorbance wavelength of avian SWS1 opsin visual pigments. J Comp Physiol A Neuroethol Sens Neural Behav Physiol 195: 167–173.

Ödeen A, Håstad O (2003): Complex distribution of avian color vision systems revealed by sequencing the SWS1 opsin from total DNA. Mol Biol Evol 20:855–861.

Ödeen A, Håstad O, Alström P (2011): Evolution of ultraviolet vision in the largest avian radiation – the passerines. BMC Evol Biol 11:313.

O'Rourke CT, Hall MI, Pitlik T, Fernández-Juricic E (2010): Hawk eyes I: diurnal raptors differ in visual fields and degree of eye movement. PLoS One 5:e12802.

Osorio D, Miklosi A, Gonda Z (1999): Visual ecology and perception of coloration patterns by domestic chicks. Evol Ecol 13:673–689.

Pettigrew JD, Dreher B, Hopkins CS, McCall MJ, Brown M (1988): Peak density and distribution of ganglion-cells in the retinae of Microchiropteran bats – implications for visual acuity. Brain Behav Evol 32:39–56.

Popp JW (1988): Effects of food-handling time on scanning rates among American goldfinches. Auk 105:384–385.

Querubin A, Lee HR, Provis JM, O'Brien KMB (2009): Photoreceptor and ganglion cell topographies correlate with information convergence and high acuity regions in the adult pigeon *(Columba livia)* retina. J Comp Neurol 517:711–722.

Rahman ML, Aoyama M, Sugita S (2007): Regional specialization of the tree sparrow *Passer montanus* retina: ganglion cell density and oil droplet distribution. Ornithol Sci 6:95–105.

Rahman ML, Aoyama M, Sugita S (2008): Ganglion cell density and oil droplet distribution in the retina of the brown-eared bulbul *(Hypsipetes amaurotis).* Anat Sci Int 83:239–246.

Rahman ML, Sugita S, Aoyama M, Sugita S (2006): Number, distribution and size of retinal ganglion cells in the jungle crow *(Corvus macrorhynchos).* Anat Sci Int 81:253–259.

Reymond L (1985): Spatial visual acuity of the eagle *Aquila audax:* a behavioural, optical and anatomical investigation. Vision Res 25: 1477–1491.

Reymond L (1987): Spatial visual acuity of the falcon *Falco berigora*: a behavioural, optical and anatomical investigation. Vision Res 27: 1859–1874.

Shi Y, Yokoyama S (2003). Molecular analysis of the evolutionary significance of ultraviolet vision in vertebrates. Proc Natl Acad Sci USA 100:8308–8313.

Slomianka L, West MJ (2005): Estimators of the precision of stereological estimates: an example based on the CA1 pyramidal cell layer of rats. Neuroscience 136:757–767.

Stone J (1981): The Wholemount Handbook: a Guide to the Preparation and Analysis of Retinal Wholemounts. Sydney, Maitland.

Tisdale V, Fernández-Juricic E (2009): Vigilance and predator detection vary between avian species with different visual acuity and coverage. Behav Ecol 20:936–945.

Tovée MJ (1995): Ultra-violet photoreceptors in the animal kingdom: their distribution and function. Trends Ecol Evol 10:455–460.

Tucker VA (2000): The deep fovea, sideways vision and spiral flights paths in raptors. J Exp Biol 203:3745–3754.

Ullmann JFP, Moore BA, Temple SE, Fernández-Juricic E, Collin SP (2012): The retinal wholemount technique: a window to understanding the brain and behaviour. Brain Behav Evol 79:26–44.

von Campenhausen M, Kirschfeld K (1998): Spectral sensitivity of the accessory optic system of the pigeon. J Comp Phys A Neuroethol Sens Neural Behav Physiol 183:1–6.

Walls GL (1942): The visual cells and their history. Biol Symp 7:203–251.

West MJ, Slomianka L, Gundersen HJG (1991): Unbiased stereological estimation of the total number of neurons in the subdivisions of the rat hippocampus using the optical fractionator. Anat Rec 231:182–497.

Williams DR, Coletta NJ (1987): Cones spacing and the visual resolution limit. J Opt Soc Am A 4:1514–1523.